Crystallization of $Al_{87}Y_5Ni_8$ amorphous alloys doped with Dy and Fe

Taras MIKA[1*], Malgorzata KAROLUS[2], Lidiya BOICHYSHYN[1], Grzegorz HANECZOK[2], Bohdan KOTUR[1], Viktor NOSENKO[3]

[1] *Faculty of Chemistry, Ivan Franko National University of Lviv, Kyryla i Mefodiya St. 6, 79005 Lviv, Ukraine*
[2] *Institute of Material Science, University of Silesia, Bankowa 12, 40-007 Katowice, Poland*
[3] *Kurdyumov Institute for Physics of Metals, NAS of Ukraine, Vernadsky Ave. 36, 03680 Kyiv, Ukraine*
* Corresponding author. E-mail: mikat@ukr.net

Amorphous alloys have been investigated by applying differential scanning calorimetry (DSC), X-ray diffraction (XRD) and high resolution electron microscopy (HREM). Replacement of Y by Dy shifts the primary crystallization to lower temperatures, substitution of Fe for Ni shifts the nanocrystallization to higher temperatures. The *RE* elements play a dominant role at the first stage of crystallization, the *TM* elements take part in the crystallization only at the final stage. For alloys with Dy the first two stages of crystallization are attributed to the formation of fcc Al(*RE*). At the third stage of crystallization, precipitation of the ternary compound $RE_3Ni_5Al_{19}$ with an orthorhombic $Gd_3Ni_5Al_{19}$-type structure was observed. The interaction between Dy and Fe atoms completely changes the crystallization path of the $Al_{87}Dy_5Ni_4Fe_4$ alloy, *i.e.* primary crystallization is attributed to precipitation of unidentified intermetallic compounds and the following stages to the formation of intermetallics isotypic with $CeMn_4Al_8$ and $YbFe_2Al_{10}$.

X-ray diffraction / Aluminium alloys / Amorphous alloys / Nanostructured materials / Phase transformation

Introduction

Amorphous metallic alloys (AMA), and especially Al–*RE*–*TM* (*RE* = rare-earth metal, *TM* = transition metal) Al-based alloys, attract interest because of their remarkable properties, such as good ductility and corrosion resistance [1,2]. It is a well-known fact that nanocrystallization can improve the corrosion resistance and mechanical properties of Al-based AMAs. Understanding the processes of primary crystallization helps controlling the nanocrystallization and may, consequently, improve the properties. The alloys of the Al–Y–Ni ternary system have relatively broad ranges of existence of the amorphous state in comparison with other Al–*RE*–*TM* systems [1]. That is why the investigation of this system is attractive for doping its alloys with other elements in a broad range and evaluating the influence on the thermal stability and other characteristics.

There is a large amount of data in the literature on the crystallization of Al–*RE*–*TM* amorphous alloys. The $Al_{85}Y_xNi_{15-x}$ (x = 5, 7, 8, 10) AMAs undergo three stages of crystallization for the alloys with x = 5, 7 and four stages for x = 8, 10 [3]. For the alloys with x = 5, 7, 8, Al nanocrystals were observed after the first stage of crystallization. An unknown intermetallic compound (IMC) crystallized after heat treatment of the $Al_{85}Y_{10}Ni_5$ AMA. Besides, an increase of the Y content shifts the primary crystallization to higher temperatures.

Sahoo *et al.* [4] reported two stages of crystallization for $Al_{94-x}La_xNi_6$ (x = 4-7) AMAs. The primary crystallization leads to precipitation of Al (for x = 4, 5). The following stages lead to crystallization of Al and of an unknown intermetallic compound (for x = 6), or only of the unknown intermetallic compound (for x = 7). The final stage of crystallization leads to precipitation of two phases (La_3Al_{11} + $NiAl_3$) for x = 4-6 and three phases (La_3Al_{11} + $NiAl_3$ + Al) for x = 7. Gao and Shiflet [5] reported three to five stages of crystallization for $Al_{100-x-y}Gd_xNi_y$ (x = 3-12, y = 3-10). Al and an unknown IMC appeared at the first stage of crystallization of $Al_{87}Gd_{10}Ni_3$, $Al_{87}Gd_{11}Ni_3$, $Al_{85}Gd_{12}Ni_3$ and $Al_{85}Gd_8Ni_7$, while crystallization of Al was observed for the other alloys.

According to [6], the iron-containing alloy $Al_{88}Y_7Fe_5$ crystallizes in three stages with precipitation of nanoparticles of Al at the first stage. Three stages of crystallization were observed for

$Al_{90}Y_5Fe_5$, $Al_{85}Y_{7.5}Fe_{7.5}$ and $Al_{80}Y_{10}Fe_{10}$ alloys with crystallizing of an IMC at the first stage [7]. Doping of ternary alloys by a fourth component allows changing their thermal stability and other parameters. Replacement of only 1 at.% of La by Ti in an $Al_{87}La_6Ni_7$ amorphous alloy prevents crystallization of unknown intermetallic phases and leads to crystallization of Al at the first stage of crystallization [8]. Replacement of 1 at.% of Ni by Cu in the $Al_{88}Sm_4Ni_8$ AMA shifts the primary crystallization of Al by about 17 K to higher temperatures [9]. Yang *et al.* [10] reported three stages of crystallization for $Al_{85}Y_{8-x}Ni_5Co_2Fe_x$ (x = 0-5) with precipitation of Al at the 1-st and 2-nd stages for x = 0, 2 and of binary and ternary intermetallic compounds (also metastable) for other alloys.

Analysis of [1-10] reveals that an increase of the content of rare-earth and/or transition metal element has a complex influence on the thermal stability and phase content of the alloys after crystallization. Summarizing the data presented above one can conclude that crystallization of AMAs strongly depends on the AMA content and is a complex process that needs additional investigations.

In our recent investigation [11] it was shown that partial substitution of Fe for Ni in the $Al_{87}Y_5Ni_8$ alloy slows down the diffusion of Al atoms and shifts the crystallization to higher temperatures, while partial replacing of Y by Gd has the opposite effect.

The aim of the present work was to study the doping effect of another *RE*, Dy, and of the 3*d*-element Fe on the thermal stability of the $Al_{87}Y_5Ni_8$ amorphous alloy. We will also focus on the thermal stability and crystallization process of the AMA as a function of the quantity of doping elements.

Experimental procedure

The basic amorphous alloy $Al_{87}Y_5Ni_8$ and three other alloys: $Al_{87}Dy_5Ni_8$, $Al_{87}Y_4Dy_1Ni_8$ and $Al_{87}Dy_5Fe_8$, were prepared by the melt spinning technique in helium atmosphere, in the form of ribbons with a thickness of about 60 μm and a width of 15 mm. The melt was prepared from pure metals and binary *RE*Al₃ (*RE* = Y, Dy) compounds. The purities of the initial metals were the following: Al – 99.999 wt.%, Ni – 99.99 wt.%, Fe – 99.99 wt.%, Y – 99.96 wt.%, and Dy – 99.99 wt.%. Rare-earth metals in the form of binary compounds *RE*Al₃ were primarily obtained by the arc-melting technique from metals of the same purity.

In order to study the crystallization of the above mentioned alloys the following experimental techniques were used:

1. Differential scanning calorimetry (DSC, Perkin-Elmer Pyris 1). The samples (about 15 mg) were encapsulated in aluminum capsules and heated up to 850 K at heating rates of 10, 15 and 20 K/min. As reference plate the same empty aluminum capsule was

used. The data were evaluated by applying the standard program Pyris.

2. X-ray diffraction (XRD, X'-Pert Philips PW 3040 diffractometer, Cu K_α radiation with a monochromator on the reflected beam, 2θ range: 10-140°, scanning step: 0.04°). This method was used for samples in the as-quenched state and annealed at elevated temperatures. Annealing was carried out for samples sealed into evacuated quartz tubes and heated at a heating rate of 20 K/min up to the temperature corresponding to the end of the DSC peak, and then quenched in water. In order to determine the structure of the examined material, the Rietveld method was used (standard FullProf and PCW programs) [12,13]. X-ray diffraction data was also used for the calculation of the average crystallite size (±20 %) by the Williamson-Hall method [14].

3. High-resolution electron microscopy (HREM, JEM 3010 electronic microscope). The microscopic observations were used in order to confirm (or not) the data obtained by the DSC and XRD techniques.

Results and discussion

Fig. 1 presents X-ray diffraction patterns obtained for the examined alloys in the as-quenched state. The profile confirms the amorphous state of the initial alloys.
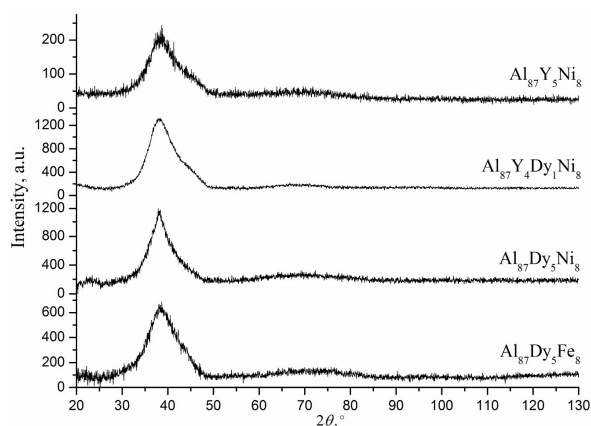

Fig. 1 XRD patterns of the initial amorphous alloys with Dy (Cu K_α).

3.1 DSC study of amorphous alloys

Fig. 2 presents DSC curves obtained for the amorphous alloys containing Dy with a heating rate of 20 K/min. The Fe-free alloys crystallize in three stages. The first maximum, corresponding to the primary crystallization of the AMA, takes place in the temperature range 442-527 K.

Partial replacement of Y by Dy (1 at.%) causes a shift of the first DSC maximum to lower temperatures by 22 K, which can be interpreted as a reduction of the thermal stability of the AMA. Complete substitution of Dy for Y decreases the temperature of primary

crystallization by another 21 K. Replacement of 8 at.% of Ni by Fe severely changes the shape of the DSC curve and improves the thermal stability of the AMA by more than 100 K. This alloy crystallizes in 5 stages. The last DSC maximum, at about 780 K, is very broad and shallow in comparison with the other ones, as it is seen from Fig. 2b. Characteristic temperatures of the DSC maxima are presented in Table 1.

In our previous work [11] on $Al_{87}RE_5TM_8$ alloys with RE = Y, Gd we did not present results on the activation energy of crystallization of the amorphous alloys. These results are presented in the present work, discussed in details and compared with those obtained for the Dy-containing AMAs.

The activation energy was determined according to the Kissinger equation [15] for heating rates of 10, 15 and 20 K/min from the slope of the curve $\ln(b/T_p)$ *vs.* $1/T_p$; where b is the heating rate and T_p is the maximum temperature of the peak . These curves, plotted in Fig. 3 for each of the exothermic reactions, show linear dependencies. The activation energies were determined from the Kissinger plots for all the investigated alloys (see Table 2).
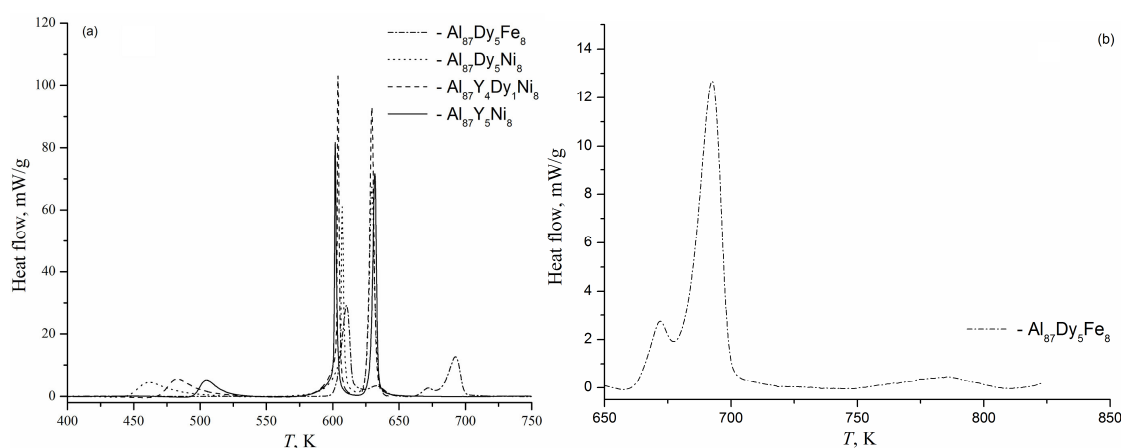

Fig. 2 (a) DSC curves for $Al_{87}RE_5TM_8$ (RE = Y, Dy; TM = Fe, Ni) amorphous alloys obtained at a heating rate of 20 K/min; (b) final stages (III, IV and V) of crystallization of the $Al_{87}Dy_5Fe_8$ AMA.

Table 1 The characteristic temperatures of the DSC curves of AMAs: T_{1max}, T_{2max}, T_{3max}, T_{4max}, T_{5max} are the maximum temperatures of the first, second, third, fourth, and fifth exothermal peaks.

AMA	T_{1max}, K	T_{2max}, K	T_{3max}, K	T_{4max}, K	T_{5max}, K
$Al_{87}Y_5Ni_8$ [a]	505	602	632	–	–
$Al_{87}Y_4Dy_1Ni_8$	483	604	630	–	–
$Al_{87}Dy_5Ni_8$	462	607	629	–	–
$Al_{87}Dy_5Fe_8$	611	633	672	693	786

[a] data taken from [11]

Table 2 Activation energy $E_{a,1-5}$ corresponding to the crystallization stages of $Al_{87}RE_5TM_8$ (RE = Y, Gd, Dy; TM = Fe, Ni) amorphous alloys (in kJ/mol).

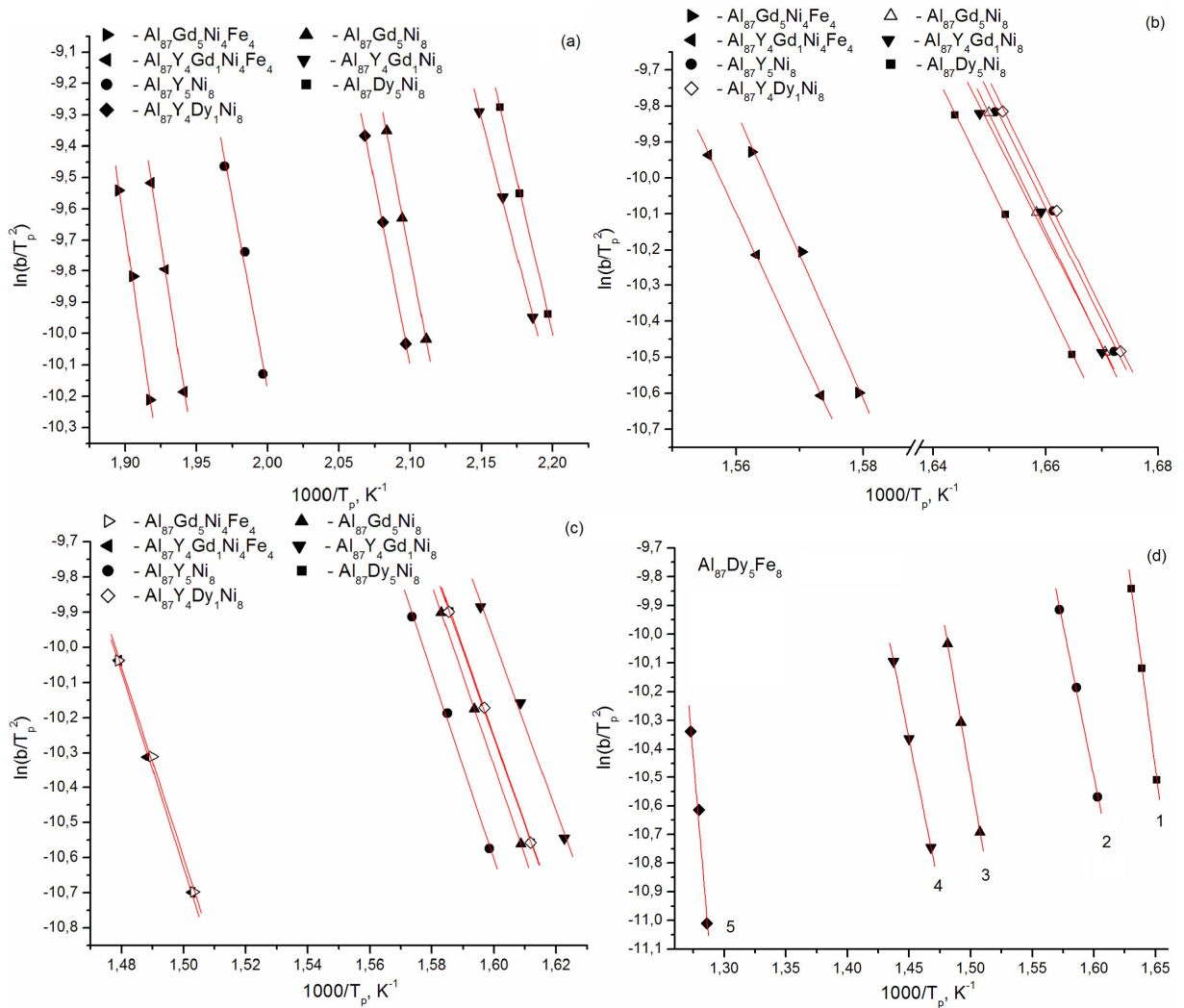| AMA	$E_{a,1}$	$E_{a,2}$	$E_{a,3}$	$E_{a,4}$	$E_{a,5}$
$Al_{87}Y_5Ni_8$	203±29	261±24	221±12	–	–
$Al_{87}Y_4Gd_1Ni_8$	146±5	255±27	204±15	–	–
$Al_{87}Gd_5Ni_8$	199±5	268±1	213±1	–	–
$Al_{87}Gd_5Ni_4Fe_4$	256±15	333±21	227±8	–	–
$Al_{87}Y_4Gd_1Ni_4Fe_4$	241±5	317±5	233±6	–	–
$Al_{87}Y_4Dy_1Ni_8$	194±5	265±13	207±6	–	–
$Al_{87}Dy_5Ni_8$	163±2	267±5	209±2	–	–
$Al_{87}Dy_5Fe_8$	267±1	176±7	207±1	178±1	420±51

Fig. 3 Kissinger plots for the first (a), second (b) and third (c) exothermic DSC peaks for the Ni-containing $Al_{87}RE_5TM_8$ (RE = Y, Gd, Dy; TM = Fe, Ni) alloys and for the five DSC exothermic peaks (1-5) for the $Al_{87}Dy_5Fe_8$ amorphous alloy (d).

3.2 XRD and HREM study of alloys

In order to study the primary crystallization of the AMAs the examined samples were sealed into evacuated quartz tubes and were heated at a heating rate of 20 K/min to the temperature of the end of the first DSC maximum, and then quenched in water. The obtained XRD patterns for the $Al_{87}Y_4Dy_1Ni_8$ and $Al_{87}Dy_5Ni_8$ alloys are presented in Fig. 4.

According to the XRD data the first stage of crystallization can be attributed to formation of Al nanograins. Analysis of the XRD spectra obtained for these samples shows that the unit cell parameters of the observed Al phase in both cases are slightly larger than for pure Al (0.40494 nm): 0.4056(1) nm for $Al_{87}Dy_5Ni_8$ and 0.40522(7) nm for $Al_{87}Y_4Dy_1Ni_8$. This probably means that the heat treatment causes formation of a solid solution Al(RE). However, this fact does not object to the possible segregation of RE-elements at the Al-nanocrystals/amorphous matrix boundaries, as reported by Hono *et al.* [16].

Additional examinations were performed on samples annealed for 1 h at 518 K for $Al_{87}Dy_5Ni_8$ and 527 K for $Al_{87}Y_4Dy_1Ni_8$. Fig. 5 presents results for the 1 h-heat treated $Al_{87}Dy_5Ni_8$ AMA. One can notice that Al(RE) nanograins (dark black, approximate size 20 nm) are scatted randomly in an amorphous matrix. The crystallite sizes calculated from the XRD data by applying the Williamson-Hall method are close to those obtained from the HREM data (see Table 3). The volume fractions of the Al nanocrystalline phase after different stages of crystallization are also presented (see Table 4).

One can see dark grains of Al(RE) on Fig. 5 and both light and gray regions of amorphous matrix. Such splitting of the amorphous matrix into two parts could be related to different distributions of rare-earth elements. Another possibility could concern the formation of primary and secondary induced Al-nanocrystals after 1 h heat treatment. If this is true, the three fields (primary and secondary Al-
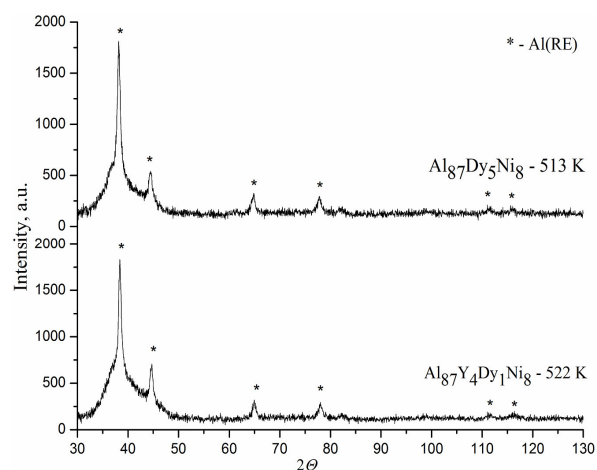
Fig. 4 XRD patterns of amorphous alloys heated up to different temperatures after having reached the first stage of crystallization.
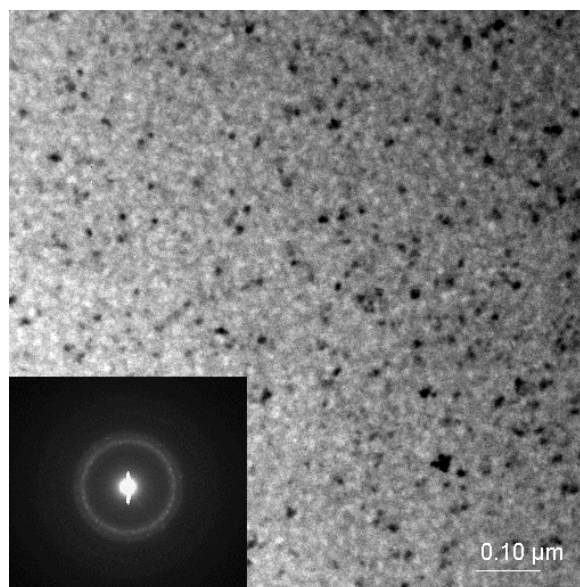

Fig. 5 HREM image of the Al$_{87}$Dy$_5$Ni$_8$ AMA heat-treated at 518 K for 1 h.

Table 3 The crystallite size (*D*) and average microstrain ($\varepsilon \pm 0.5$) of the Al(*RE*) grains for Al$_{87}$Y$_{5-x}$Dy$_x$Ni$_8$ (x = 0, 1, 5) AMAs heated at 20 K/min to the annealing temperature T_{ann}.

AMA	I-st stage of crystallization			II-nd stage of crystallization		
	Annealing temperature T_{ann}, K	Crystallite size D, nm	Microstrain, %	Annealing temperature T_{ann}, K	Crystallite size D, nm	Microstrain, %
Al$_{87}$Y$_5$Ni$_8$	512	15	2	612	30	2
Al$_{87}$Y$_4$Dy$_1$Ni$_8$	522	20	3	615	60	3
Al$_{87}$Dy$_5$Ni$_8$	513	25	2	618	35	2

Table 4 The volume fraction of nanocrystals after stage I and II of crystallization.

AMA	Volume fraction of Al(*RE*) nanocrystals (± 0.05)	
	I-st stage	II-nd stage
Al$_{87}$Y$_5$Ni$_8$	0.28	0.39
Al$_{87}$Y$_4$Dy$_1$Ni$_8$	0.32	0.45
Al$_{87}$Dy$_5$Ni$_8$	0.34	0.51

nanocrystals and the remaining amorphous matrix) are observed on the HREM image.

XRD spectra of the amorphous alloys containing Dy, heated up to temperatures after the second DSC peak, are shown in Fig. 6. The patterns are similar: in all the cases Al diffraction lines and diffuse scattering (which is attributed to the remaining amorphous matrix) are observed.

X-ray diffraction patterns obtained for the Al$_{87}$Dy$_5$Ni$_8$ and Al$_{87}$Y$_4$Dy$_1$Ni$_8$ AMAs after the third stage of crystallization are presented in Fig. 7. For these alloys it is the final stage of crystallization. The XRD patterns contain reflections from two phases: Al(*RE*) solid solution and a ternary

compound *RE*$_3$Ni$_5$Al$_{19}$ with Gd$_3$Ni$_5$Al$_{19}$-type structure [17].

As can be seen from Table 5, the lattice parameters of the Al grains, refined from the XRD patterns, decrease from the first to the third stages of crystallization, but in all cases they are larger than for pure Al (0.40494 nm), which could indicate the formation of a solid solution Al(*RE*). The decrease of the lattice parameters of Al(*RE*) could be related to the formation of pure Al-nanocrystals at the second stage of crystallization.

Results of the Rietveld profile refinement of the XRD data for the Al$_{87}$Dy$_5$Ni$_8$ alloy are presented in Fig. 8. The XRD profile and the refined cell

parameters for the $Dy_3Ni_5Al_{19}$ intermetallic compound (a = 0.40685(5) nm, b = 1.5941(2) nm, c = 2.6975(3) nm) are in good agreement with literature data: a = 0.40893(7) nm, b = 1.5993(2) nm, c = 2.7092(4) nm [17].

The crystallization path of the $Al_{87}Dy_5Fe_8$ alloy differs completely from those of the two other investigated Dy-alloys, as can be seen from Fig. 9. Crystallization occurs in 5 stages. The first stage of crystallization is attributed to the formation of an unidentified intermetallic compound (or compounds). It is marked as σ-phase. After the second stage of
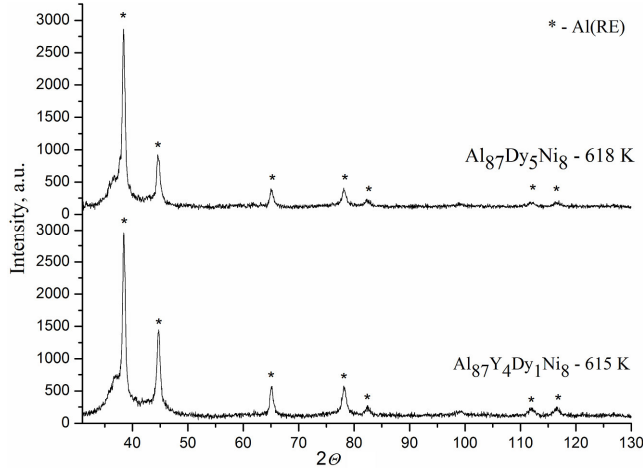
crystallization the AMA consists of Al(Dy), the IMC $DyFe_4Al_8$ with $CeMn_4Al_8$-type structure and the unidentified compound (σ-phase) from the previous stage of crystallization. The third stage of crystallization is attributed to the formation of Al(Dy) and the IMC $DyFe_4Al_8$. The σ-phase decomposes, while traces of another unidentified IMC (μ-phase) appear in the XRD pattern. The XRD patterns corresponding to the fourth and fifth stage of crystallization indicate the following phase content: Al(Dy), the IMC $DyFe_2Al_{10}$ with $YbFe_2Al_{10}$-type structure and the μ-phase. The fourth stage of

Fig. 6 XRD patterns of amorphous alloys heated up to different temperatures after having reached the second stage of crystallization.
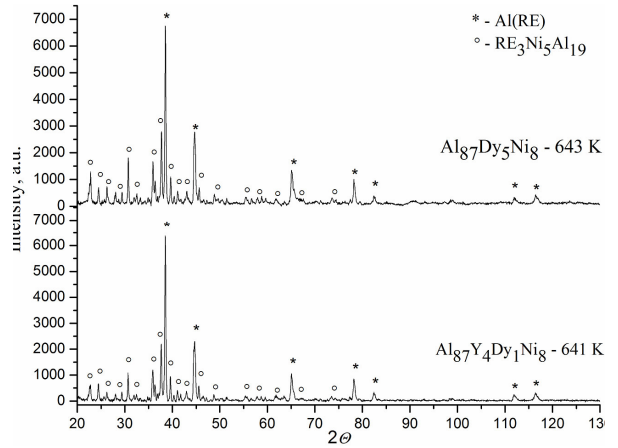
Fig. 7 XRD patterns of amorphous alloys heated up to different temperatures after having reached the third stage of crystallization.

Fig. 8 XRD pattern obtained for the $Al_{87}Dy_5Ni_8$ alloy after the third stage of crystallization and results of the Rietveld refinement (dots and line are experimental and theoretical data, respectively; the difference diagram is shown at the bottom; * – Al(*RE*), ○ – $Dy_3Ni_5Al_{19}$, residuals R_p = 3.29%, R_{wp} = 4.24%, GoF = 1.19).
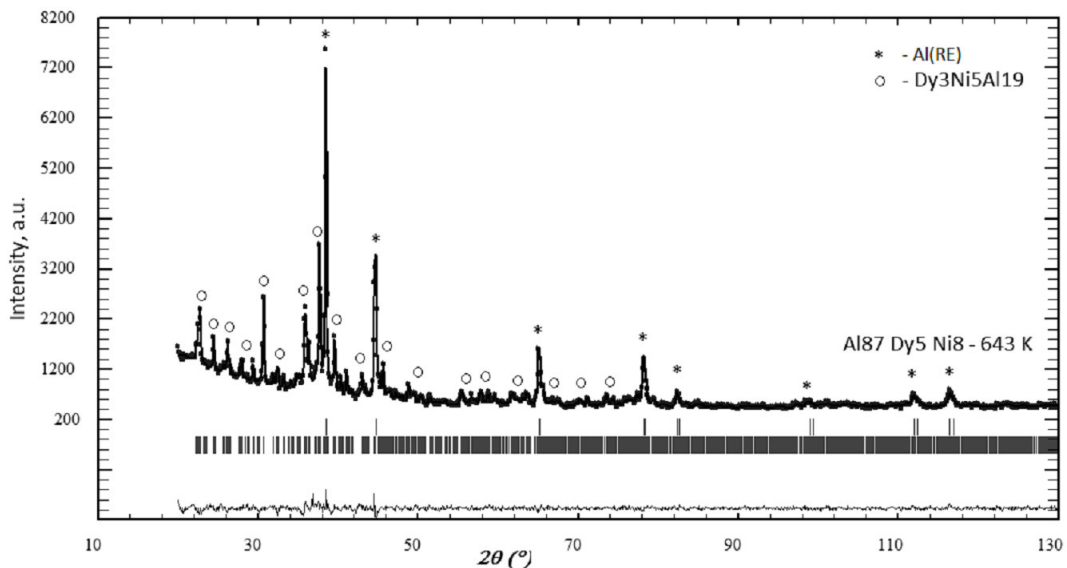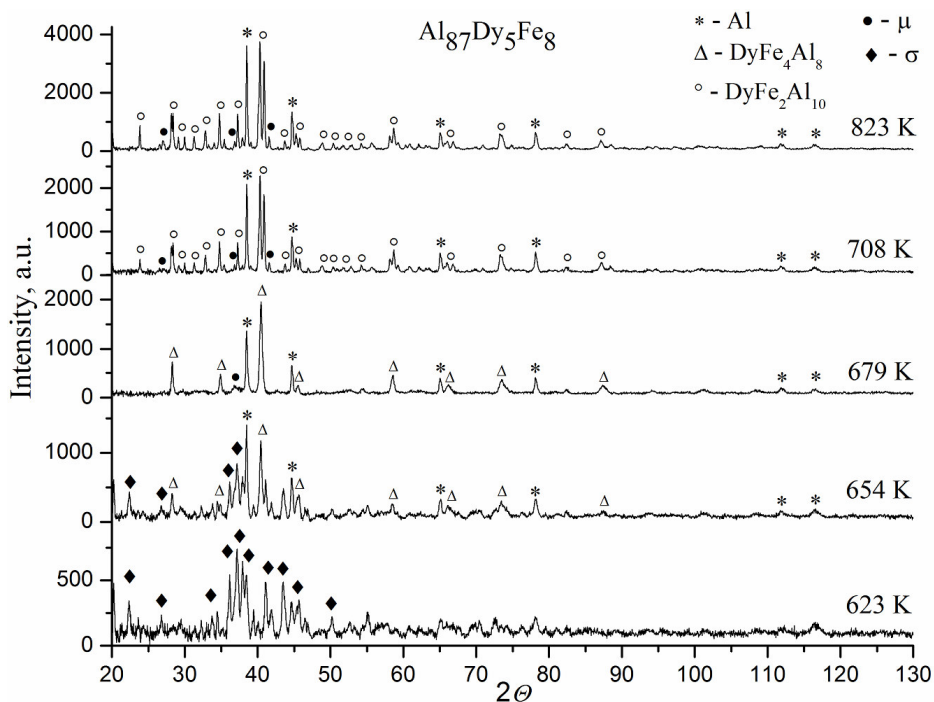
Fig. 9 XRD patterns of $Al_{87}Dy_5Fe_8$ amorphous alloys heated up to different temperatures after 1-5 stages of crystallization.

Table 5 Lattice parameters of Al(*RE*) after stage I, II and III of crystallization (in nm).

AMA	I-st stage	II-nd stage	III-rd stage
$Al_{87}Y_5Ni_8$[a]	0.4059(2)	0.4055(1)	0.40522(6)
$Al_{87}Y_4Dy_1Ni_8$	0.4061(3)	0.40557(7)	0.40527(4)
$Al_{87}Dy_5Ni_8$	0.4064(2)	0.40544(5)	0.40518(3)

[a] data taken from [11]

crystallization probably corresponds to decomposition of the $DyFe_4Al_8$ intermetallic compound. The last exothermic effect is very small (see Fig. 2b). Based on this, one can conclude that the last (fifth) exothermic DSC maximum for the $Al_{87}Dy_5Fe_8$ amorphous alloy corresponds to crystallization of the remaining amorphous phases, with the same products of crystallization as mentioned earlier.

The last crystallization stage of the Fe-free $Al_{87}RE_5Ni_8$ alloys occurs in the temperature range 621-639 K, while for the $Al_{87}Dy_5Fe_8$ alloy this temperature range is considerably higher: 750-808 K (see Fig. 2). Partial replacement of Y by Dy ($Al_{87}Y_5Ni_8 \rightarrow Al_{87}Y_4Dy_1Ni_8$) shifts T_{1max} to lower temperatures by about 20 K (see Table 1). Total replacement of Y by Dy ($Al_{87}Y_5Ni_8 \rightarrow Al_{87}Dy_5Ni_8$) causes an additional shift of this maximum by 22 K. As reported previously [11], the doping effect of another *RE*, Gd, is similar. Partial substitution of Gd for Y ($Al_{87}Y_5Ni_8 \rightarrow Al_{87}Y_4Gd_1Ni_8$) shifts the crystallization to lower temperatures (from 505 K to

462 K) and total substitution of Gd for Y ($Al_{87}Y_5Ni_8 \rightarrow Al_{87}Gd_5Ni_8$) shifts it down to 478 K.

As it can be seen from Table 2, partial and complete substitution of Fe for Ni causes a significant increase of the activation energy $E_{a,1}$ with respect to the basic alloy $Al_{87}Y_5Ni_8$. Partial replacement of Y by Gd has the opposite effect (the activation energy $E_{a,1}$ decreases significantly), but complete replacement of Y by Gd causes almost no further change of $E_{a,1}$. Partial replacement of Y by Dy causes minor changes of E_{a1}, while the complete replacement of Y by Dy reduces it significantly.

The second crystallization stage is characterized by approximately the same activation energy $E_{a,2}$ for all the alloys containing no Fe, approximately 265-270 kJ/mol. For the alloys containing Fe (except the $Al_{87}Dy_5Fe_8$ alloy), $E_{a,2}$ is also approximately the same. For the third (and final) stage of crystallization of the investigated AMAs there are similar tendencies as for the second stage: the value of the activation energy is approximately the same for all the alloys
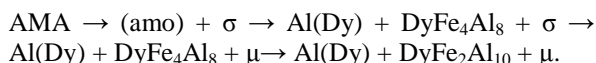
without Fe and is equal to ~210-220 kJ/mol whereas for the alloys with Fe it is slightly higher, ~230 kJ/mol.

Comparing the crystallization temperature, activation energy of crystallization and phase content for different AMAs (except the $Al_{87}Dy_5Fe_8$ alloy), it can be seen (Table 1) that doping of the reference $Al_{87}Y_5Ni_8$ alloy by other *RE* elements reduces the temperature of primary crystallization, while Fe-doping increases it considerably. It should also be noted that the values of the activation energy of the second stage of crystallization (Table 2) are almost the same and do practically not depend on the *RE* element. This means that the *RE* elements play a key role at the first stage of crystallization. The X-ray analysis shows the formation of an Al(*RE*) solid solution at the first two stages of crystallization for the Ni-containing alloys. These results can be interpreted as formation of Al(*RE*) nanocrystals from an amorphous matrix at the first stage of crystallization and thermally induced crystallization at the second stage of crystallization (when additional energy of nucleation is needed). Contrary to the doping effect of the *RE*, Fe slows down the diffusion of atoms at all crystallization stages and takes part in the crystallization only at the final stages.

The crystallization path of the $Al_{87}Dy_5Fe_8$ amorphous alloy differs completely from those of the Ni-containing alloys. Its crystallization occurs in 5 stages. It may be noted that the similar alloy with Ni, $Al_{87}Dy_5Ni_8$ crystallizes in three stages.

The atomic ratio of the transition and rare-earth metal is almost the same for the amorphous alloys $Al_{87}RE_5Ni_8$ (*TM:RE* = 1:0.625) and the crystallized ternary IMC $RE_3Ni_5Al_{19}$ (*TM:RE* = 1:0.6). For the crystallization of the IMC from the amorphous matrix there is an excess of Al and a small excess of *RE* in the $Al_{87}RE_5Ni_8$ AMA, which crystallizes as a solid solution Al(*RE*). The composition of the $Al_{87}Y_5Ni_8$ alloy corresponds to the two-phase equilibrium $<Al + Y_3Ni_5Al_{19}>$, according to the equilibrium phase diagram of the ternary system Y–Ni–Al [18]. The crystallization path of this amorphous alloy occurs by an equilibrium mechanism and corresponds to the Y–Ni–Al phase diagram.

According to the XRD results the crystallization path of the $Al_{87}Dy_5Fe_8$ amorphous alloy can be described by the following scheme:

$$AMA \rightarrow (amo) + \sigma \rightarrow Al(Dy) + DyFe_4Al_8 + \sigma \rightarrow$$
$$Al(Dy) + DyFe_4Al_8 + \mu \rightarrow Al(Dy) + DyFe_2Al_{10} + \mu.$$

As it was described earlier, the ratio between the content of transition metal and rare-earth metal for the amorphous alloy $Al_{87}Dy_5Fe_8$ (*TM:RE* = 1:0.625) is higher than for the crystalline IMCs $DyFe_4Al_8$ (*TM:RE* = 1:0.25) and $DyFe_2Al_{10}$ (*TM:RE* = 1:0.5). So, it is possible to deduce that the σ-phase, which appears at the first stage of crystallization, is a phase containing a larger amount of rare-earth metal. The

second stage of crystallization is attributed to decomposition of the amorphous matrix (amo) into Al(Dy) and $DyFe_4Al_8$. The following (3-rd) stage of crystallization corresponds to decomposition of the rare-earth rich σ-phase into Al(Dy), a residual unidentified IMC (μ-phase) and $DyFe_4Al_8$. The fourth stage of crystallization is attributed to decomposition of the IMC $DyFe_4Al_8$ into $DyFe_2Al_{10}$, Al(Dy) and μ-phase. The IMC $DyFe_2Al_{10}$ contains twice less Fe than $DyFe_4Al_8$, and the excess of Fe probably crystallizes as a Fe-rich intermetallic compound (μ).

Investigations for the identification of the σ- and μ-phases are in progress.

Conclusions

Thermally induced crystallization of $Al_{87}Y_5Ni_8$ amorphous alloys doped with Dy and Fe has been investigated.

The Ni-containing alloys $Al_{87}Y_4Dy_1Ni_8$ and $Al_{87}Dy_5Ni_8$ crystallize in 3 stages. Replacement of Y by Dy(Gd) shifts the primary crystallization to lower temperatures and decreases the crystallization activation energy. The *RE* elements play a dominant role at the first stage of crystallization. The first two stages of crystallization of the AMAs without Fe were attributed to the formation of nanograins of Al(*RE*) solid solution. At the third, final stage, precipitation of the ternary compounds $RE_3Ni_5Al_{19}$ with orthorhombic $Gd_3Ni_5Al_{19}$-type structure occurs.

The Fe-containing amorphous alloy $Al_{87}Dy_5Fe_8$ crystallizes in 5 stages. Fe-doping slows down the diffusion of Al atoms in the amorphous matrix and increases the thermal stability of the amorphous alloys by about 100 K and increases the activation energy of primary crystallization. Complete crystallization of the $Al_{87}Dy_5Fe_8$ AMA leads to the formation of two unidentified intermetallic compounds (σ and μ) and two other IMC with $CeMn_4Al_8$- and $YbFe_2Al_{10}$-type structures.

References

[1] A. Inoue, *Progr. Mater. Sci.* 43 (1998) 365-520.
[2] L. Battezzati, S. Pozzovivo, P. Rizzi, In: H.S. Nalwa (Eds.), *Nanoclusters and Nanocrystals*, Am. Sci. Publ., 2003, pp. 283-309.
[3] S. Saini, A. Zaluska, Z. Altounian, *J. Non-Cryst. Solids* 250-252 (1999) 714-718.
[4] K.L. Sahoo, M. Wollgarten, J. Haug, J. Banhart, *Acta Mater.* 53 (2005) 3861-3870.
[5] M.C. Gao, G.J. Shiflet, *Scr. Mater.* 53 (2005) 1129-1134.

[6] J.C. Foley, D.R. Allen, J.H. Perepezko, *Scr. Mater.* 35(5) (1996) 655-660.

[7] Q. Li, E. Johnson, A. Johansen, L. Sarhold-Kristensen, *J. Mater. Res.* 7 (1992) 2756-2764.

[8] L. Battezzati, M. Kusy', P. Rizzi, V. Ronto', *J. Mater. Sci.* 39 (2004) 3927-3934.

[9] Y. Zhang, P.J. Warren, A. Cerezo, *Mater. Sci. Eng. A* 327 (2002) 109-115.

[10] H.W. Yang, S.C. Tjong, J.Q. Wang, *Mater. Sci. Eng. A* 406 (2005) 160-165.

[11] T. Mika, M. Karolus, G. Haneczok, L. Bednarska, E. Łagiewka, B. Kotur, *J. Non-Cryst. Solids* 354 (2008) 3099-3106.

[12] J. Rodriguez-Carvajal, *Program FullProf*, Lab. Léon Brillouin, 1998.

[13] W. Kraus, G. Nolge, *PowderCell*, Federal Institute for Materials Research and Testing, 1999.

[14] G.K. Williamson, W.H. Hall, *Acta Metall.* 1 (1953) 22-31.

[15] H.E. Kissinger, *Anal. Chem.* 29 (1957) 1702-1705.

[16] K. Hono, Y. Zhang, A.P. Tsai, A. Inoue, T. Sakura, *Scr. Metall. Mater.* 32(2) (1995) 191-196.

[17] R.E. Gladyshevskii, K. Cenzual, E. Parthé, *J. Solid State Chem.* 100 (1992) 9-15.

[18] T. Mika, B. Kotur, *Chem. Met. Alloys* 3 (2010) 208-219.